Inorg. Chem. **2008**, *47*, 1835−1848

Forum

Preparation and Study of a Family of Dinuclear Ru(II) Complexes That Catalyze the Decomposition of Water

Zeping Deng, Huan-Wei Tseng, Ruifa Zong, Dong Wang, and Randolph Thummel*

Department of Chemistry, 136 Fleming Building, University of Houston, Houston, Texas 77204-5003

Received June 1, 2007

An approach is developed for the four-electron oxidation of water to provide dioxygen that involves the juxtaposition of two Ru(II) centers such that a metal-bound water molecule might interact with one or both of the metals. The key element in this approach is an appropriate bridging ligand that will hold the metal assembly intact through the full redox cycle. Various synthetic approaches to such ligands are described with the ultimate preparation of four closely related bis-tridentate polypyridine-type systems in which the bridging and distal portions of the ligand are varied. All of these ligands self-assemble with two Ru(II) centers bridged by a Cl ion in the equatorial plane and four axial monodentate substituted pyridines or *N*-methylimidazoles to form the well-organized catalyst complexes. These complexes are characterized by their distinctive ^{1}H NMR spectra as well as an X-ray structure of one representative species. The photophysical and electrochemical features of these complexes are consistent with electronegativity and delocalization effects in the equatorial and axial ligands. Of the 14 complexes studied, all but 2, which each contain four axial *N*-methylimidazole ligands, catalyze the decomposition of water in the presence of excess Ce(IV) as a sacrificial oxidant at pH = 1. Both the rates of oxygen evolution and the catalyst turnover numbers (TNs) are measured. For the active catalysts, the relative rates vary from 1 to 51 and the TNs measure from 80 to 689. Various analytical methods for making these measurements are discussed, and it is found that there is an approximately linear relationship between the rate and TN. Future work will involve optimization of these systems and studies aimed at a better understanding of the mechanism.

Introduction

In the past decade, mankind has begun to appreciate more fully the delicate balance between his existence and his environment. This awareness has taken several forms. One form is the realization that current energy resources will not be sufficient to provide for rapidly expanding populations and emerging economies. Most important in this regard is the finite limitation of fossil fuel resources. These resources were accumulated over millions of years and thus are not renewable in any realistic sense. Another major emerging concern is the effect that our current utilization of natural resources, such as petroleum, is having on the atmosphere and general environment of our planet.

A variety of scenarios have been suggested to deal with these far-reaching issues. To a considerable extent, the energy and environment issues are linked to one another, and effective solutions to either problem must not neglect impact on the other. In this regard, the eventual movement to a hydrogen-based economy is particularly promising.[1] Hydrogen is a high-energy, clean-burning fuel that can potentially be derived from renewable resources. It is not yet clear how the wide-scale implementation of hydrogen as a fuel will come about, but it is almost an inevitable consequence of our search for an ideal fuel. Hydrogen-based fuel cell engines

* To whom correspondence should be addressed. E-mail: thummel@uh.edu.

(1) (a) *The Hydrogen Economy*; The National Academies Press: Washington, DC, 2004. (b) Sorenson, B. *Hydrogen and Fuel Cells*; Elsevier: Oxford, U.K., 2005. (c) Winter, C.-J., Nitsch, J., Eds. *Hydrogen as an Energy Carrier*; Springer-Verlag: Berlin, Germany, 1988.

10.1021/ic7010875 CCC: $40.75
Published on Web 03/10/2008

for automobiles are under active development and hydrogen fueling stations can already be found in a few highly publicized locations.[2]

An important issue that is being almost consciously avoided by those who most strongly support the development of a hydrogen economy is the source of all of the needed hydrogen. Currently, the vast majority of hydrogen is produced by thermal cracking of low molecular weight hydrocarbons: fossil fuels. Another source is the electrolysis of water, which demands more energy than it provides and where much of the electrical energy used for electrolysis comes from the burning of coal, the cause of serious atmospheric pollution. The ideal energy source that one might use for the decomposition of water would be the energy derived from sunlight. Until our sun becomes extinct, this energy source is renewable, it is pervasive throughout the planet, and it is free.

Because sunlight does not directly interact with water molecules, a photocatalyst is needed whose excited-state will possess sufficient energy to carry out the redox steps required for water decomposition. Although this perspective deals with water oxidation, both halves of the redox equation must be satisfied by a truly catalytic system. In other words, both hydrogen and oxygen must be produced, while it is, of course, hydrogen that is the useful fuel of interest.

Many existing potential photocatalysts have sufficient excited-state energy to carry out the reduction of protons and the oxidation of hydroxide, and yet none has been able to promote this process in a practical fashion. A major problem is that the water molecule often is not involved in the coordination sphere of the metal and thus internal return to the ground-state occurs before any useful photocatalysis. One way to overcome this process is to introduce water into the coordination sphere of the metal, thus involving a ground-state metal-aquo species. Two-electron oxidation of this metal-aquo to a metal-oxo species would provide a molecule of hydrogen and a species that might eventually lead to dioxygen formation.

$$M{-}OH_2 \xrightarrow{h\nu} M{=}O + H_2 \quad (1)$$

$$M{=}O + O{=}M \rightarrow O_2 + 2M \quad (2)$$

It is attractive to consider the possibility that somehow two M=O species might come together, either through O−O bridging or through the intervention of adventitious water to ultimately yield dioxygen and the starting catalyst ready for rehydration. Our objective in this study was to develop a supramolecular system that would hold two metal-bound waters in close proximity so that the chemistry depicted in eqs 1 and 2 might become more favorable.

In earlier work, we have reported the synthesis of a series of bis-tridentate bridging ligands (BLs)[3] as well as the complexation of one of these ligands with two Ru(II) atoms to afford a well-organized system **1a**−**c**, which was capable of oxidizing water in the presence of a sacrificial oxidant.[4] For this initial series of catalysts, we varied only one structural feature, the 4-substituent on the axial pyridine ligand. We noticed that this substituent had a substantial and self-consistent effect on the photophysical and electrochemical properties of the complex as well as the stability and reactivity with regards to water oxidation. In an attempt to establish further structure–activity correlations, we have prepared a family of similar dinuclear complexes in which several different domains of the molecule are varied in a regular fashion. The three domains of complex **1** that have been varied are the central linker, the peripheral binding sites, and the axial ligand. This paper will discuss the background studies that led up to the development of these oxidation catalysts as well as the synthesis of the BLs and their corresponding dinuclear complexes and the fundamental electronic properties of these systems as well as their catalytic performance.

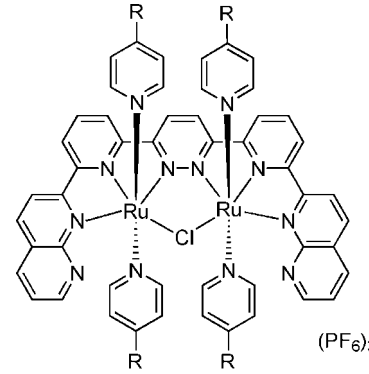

1a R = NMe_2
b R = CH_3
c R = CF_3

Background

Our interest in the development of a water oxidation catalyst originated in 1991 while the principal investigator was a sabbatical guest in the laboratories of Jean-Marie Lehn in Strasbourg, France. We were motivated by the activity of the so-called "blue dimer", which had been developed by Tom Meyer and his group[5,6] but which was plagued by cleavage of the μ-oxo bridge that held the dimer together. Our own interest in ligand design and particularly in the design of cavity-shaped polydentate ligands suggested that such a bridging species might lend stability to the blue dimer. The simplest bis-bidentate BL that would maintain the binding motif of 2,2′-bipyridine is 2,7-di(pyrid-2′-yl)pyridazine (**2**).[7]

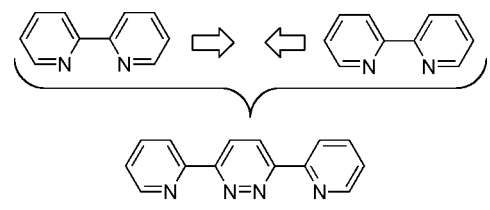

2

This interesting species is prepared in a rather unique way from the reaction of 2-cyanopyridine with hydrazine followed

(2) Sherman, D. *At Milepost 1 on the Hydrogen Highway*; New York Times: New York, Apr 28, 2007.
(3) Zong, R.; Wang, D.; Hammitt, R.; Thummel, R. P. *J. Org. Chem.* **2006**, *71*, 167–175.

Scheme 1

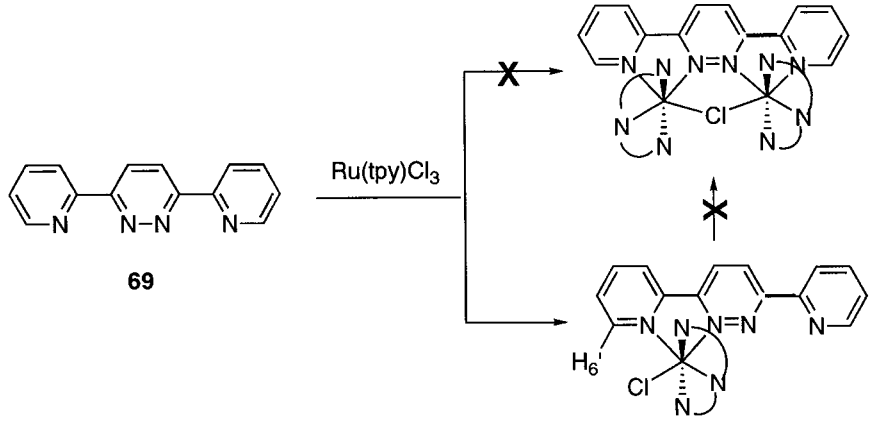

Scheme 2

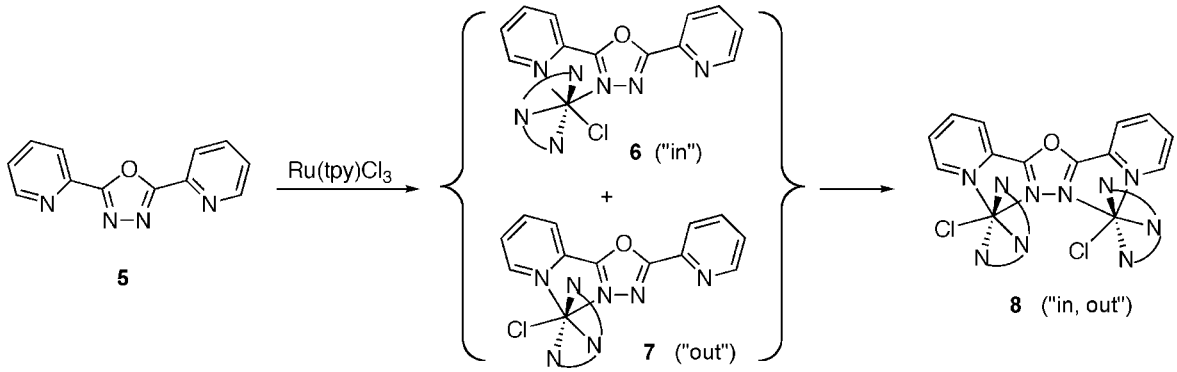

by oxidation to provide 1,2,4,5-tetrazine, which subsequently undergoes an inverse electron-demanding [2 + 4] cycloaddition with acetylene followed by extrusion of N_2 to give **2**.[5] Our intention was to introduce two $[Ru(tpy)Cl]^{2+}$ moieties (tpy = 2,2′;6′,2″-terpyridine) such that the chloro group(s) pointed "in" (**3**) and could eventually be replaced with one (or two) waters. Unfortunately, the coordination of the first Ru center occurred such that the Cl was oriented "out", providing **4**, which then prevented the desired dinuclear coordination. This orientation was clearly evident in the NMR spectrum of **4**, where H6′, instead of being shielded by the central ring of the tpy, was deshielded by the proximal Cl. It appears that the initial attack by the more basic pyridine ring of **2** on $[Ru(tpy)Cl_3]$ involves substitution of an equatorial Cl, which then sets the stereochemistry of **4**. At this point, we realized that this coordination process was, in fact, poorly understood and we undertook a careful study of the process in the hopes of remedying the problem (Scheme 1).[8]

To increase the nucleophilicity of the central ring of the BL and possibly increase its reactivity to where it could compete with the outer pyridyl ring for the initial attack on Ru, we replaced pyridazine with the more electron-rich oxadiazole. The BL **5** had been known for some time and, in fact, is derived directly from a precursor of **2**.[9] Depending on the reaction conditions, we were able to obtain products from the treatment of **5** with $[Ru(tpy)Cl_3]$ having both the "in" (**6**) and "out" (**7**) orientation of the chloro substituent. A single dinuclear product was also obtained, and from the NMR spectrum, it was tentatively assigned the "in, out" structure **8**.[10] Because of the incorrect orientation of this material as well as the very tedious nature of its preparation, requiring multiple chromatographies and ultimately providing only low yields, we suspended further work on this approach to construct a dinuclear Ru(II) catalyst (Scheme 2).

Around the year 2000, we noticed that Vince Catalano and his group at the University of Nevada, Reno were looking at the same types of bridged dinuclear Ru(II) complexes as potential oxidation catalysts. In particular, they examined dipyridyl pyridazine **2** with either a methyl or chloro substituent at the pyridyl 6′ position.[11] These workers experienced the same frustration as our group in

(4) Zong, R.; Thummel, R. P. *J. Am. Chem. Soc.* **2005**, *127*, 12802–12803.
(5) (a) Gersten, S. W.; Samuels, G. J.; Meyer, T. J. *J. Am. Chem. Soc.* **1982**, *104*, 4029–4030. (b) Gilbert, J. A.; Eggleston, D. S.; Murphy, W. R., Jr.; Geselowitz, D. A.; Gersten, S. W.; Hodgson, D. J.; Meyer, T. J. *J. Am. Chem. Soc.* **1985**, *107*, 3855–3864. (c) Chronister, C. W.; Binstead, R. A.; Ni, J.; Meyer, T. J. *Inorg. Chem.* **1997**, *36*, 3814–3815. (d) Binstead, R. A.; Chronister, C. W.; Ni, J.; Hartshorn, C. M.; Meyer, T. J. *J. Am. Chem. Soc.* **2000**, *122*, 8464–8473.
(6) Hurst, J. K. *Coord. Chem. Rev.* **2005**, *249*, 313–328.
(7) (a) Denti, G.; Sabatino, L.; De Rosa, G.; Bartolotta, A.; Di Marco, G.; Ricevuto, V.; Campagna, S. *Inorg. Chem.* **1989**, *28*, 3309–3313. (b) Butte, W. A.; Case, F. H. *J. Org. Chem.* **1961**, *26*, 4690–4692.
(8) Jahng, Y.; Thummel, R. T.; Bott, S. G. *Inorg. Chem.* **1997**, *36*, 3133–3138.
(9) Geldard, J. F.; Lions, F. *J. Org. Chem.* **1965**, *30*, 318–319.
(10) Jang, Y. Unpublished results, 1995. University of Houston, Houston, TX.
(11) (a) Catalano, V. J.; Heck, R. A.; Immoos, C. E.; Öhman, A.; Hill, M. G. *Inorg. Chem.* **1998**, *37*, 2150–2157. (b) Catalano, V. J.; Heck, R. A.; Öhman, A.; Hill, M. G. *Polyhedron* **2000**, *19*, 1049–1055.

Scheme 3

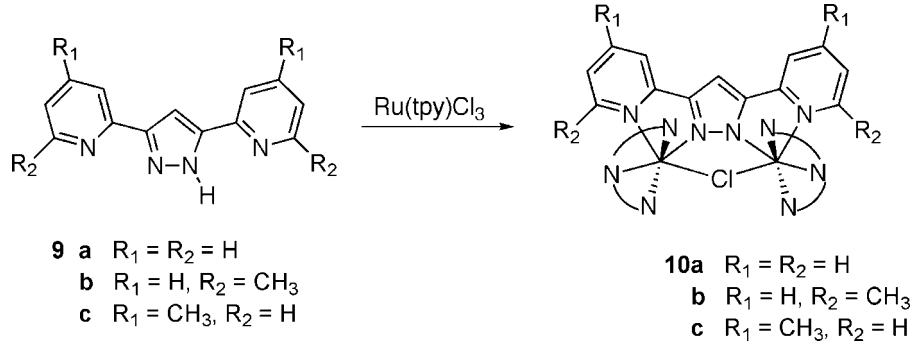

9 **a** $R_1 = R_2 = H$
b $R_1 = H$, $R_2 = CH_3$
c $R_1 = CH_3$, $R_2 = H$

10a $R_1 = R_2 = H$
b $R_1 = H$, $R_2 = CH_3$
c $R_1 = CH_3$, $R_2 = H$

Scheme 4

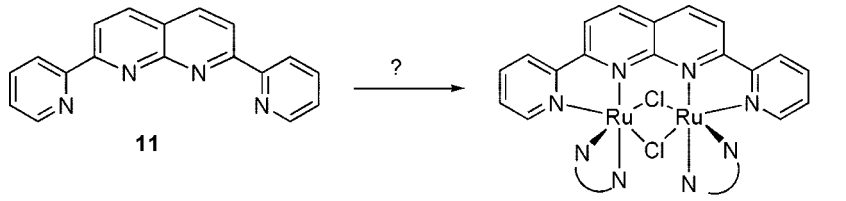

11

12 N⌒N = bpy

obtaining primarily the "out" isomer of the mononuclear complexes. However, when the methyl group was moved to the 4′ position on pyridine, some of the "in" isomer could be obtained. In a final study, they made a critical change to the BL by employing pyrazole as the linker, thus affording the parent compound **9a** as well as two dimethyl-substituted derivatives **9b** and **9c**.[12] In this series, for the methyl-substituted derivatives, they were able to obtain the desired chloro-bridged dimers **10b** and **10c** and furthermore were able to exchange the bridging group in **10b** for a variety of other species, including hydroxyl and benzoate. These systems were never tested for water oxidation (Scheme 3).[13]

In 2004, Antoni Llobet and co-workers in Spain reported on a very similar dipyridylpyrazole-bridged complex **10a** involving two Ru(tpy) moieties but lacking the methyl groups on the outer pyridyl rings.[14] These workers found that this complex was capable of acting as a catalyst for the oxidation of water to dioxygen, and this work will be reported in more detail in an accompanying perspective article from the Spanish group.[15]

In considering other possible BLs for the formation of a dinuclear Ru-based catalyst, it is worthwhile to look beyond dipyridylpyridazine, oxadiazole, and pyrazole. A simple bis-bidentate system that might be useful is 2,6-di(pyrid-2′-yl)-1,8-naphthyridine (**11**). This ligand has been known for some time and is used mostly as a BL for the construction of metal−metal-bonded systems often involving dirhodium.[16] In 1990, Kaska and co-workers reported the complex **12**, which is similar to a chloro-bridged dimer $[Ru_2Cl_2(bpy)_4]^{2+}$ reported by the Meyer group.[17] An X-ray structure for **12** was lacking so that the existence of μ-chloro bridges is somewhat questionable.[18] A Ru−Ru-bonded system might be more likely. This complex was not tested as a water oxidation catalyst (Scheme 4).

We decided to elaborate on the BL approach by going from a bis-bidentate system to a bis-tridentate bridge. In this regard, we have reported the synthesis of a series of BLs having a variety of central multidentate linker groups connecting either two 1,8-naphthyridines or two 1,10-phenanthrolines as the peripheral binding units.[3] The remainder of this report will concern the development of oxidation catalysts based on this series of ligands and the properties of these systems.

Synthesis and Characterization

In an earlier report, we described the preparation of the BL **16** in 86% yield from the Friedländer condensation of 2 equiv of 2-aminonicotinaldehyde with the diketone **13**.[3] This diketone was, in turn, prepared from the coupling of 3,6-dichloropyridazine and an appropriate stannane.

(12) (a) Catalano, V. J.; Craig, T. J. *Inorg. Chem.* **2003**, *42*, 321–334. (b) Catalano, V. J.; Kurtaran, R.; Heck, R. A.; Öhman, A.; Hill, M. G. *Inorg. Chim. Acta* **1999**, *286*, 181–188.
(13) Professor Catalano supplied us with complex **10b** and a related benzoato-bridged system, and we tested them for water oxidation. At elevated concentrations, both complexes showed modest activity with TN = 4–5.
(14) Sens, C.; Romero, I.; Rodrfíguez, M.; Llobet, A.; Parella, T.; Benet-Buchholz, J. *J. Am. Chem. Soc.* **2004**, *126*, 7798–7799.
(15) Rodrı´guez, M.; Romero, I.; Sens, C.; Llobet, A. *J. Mol. Catal. A: Chem.* **2006**, 215–220.
(16) (a) Tikkanen, W. R.; Binamira-Soriaga, E.; Kaska, W. C.; Ford, P. C. *Inorg. Chem.* **1984**, *23*, 141–146. (b) Tikkanen, W. R.; Kaska, W. C.; Moya, S.; Layman, T.; Kane, R.; Krüger, C. *Inorg. Chim. Acta* **1983**, *76*, L29–L30. (c) Thummel, R. P.; Lefoulon, F.; Williamson, D.; Chavan, M. *Inorg. Chem.* **1986**, *25*, 1675–1679.
(17) Johnson, E. C.; Sullivan, B. P.; Salmon, D. J.; Adeyemi, S. A.; Meyer, T. J. *Inorg. Chem.* **1978**, *17*, 2211–2215.
(18) Binamira-Soriaga, E.; Keder, N.; Kaska, W. C. *Inorg. Chem.* **1990**, *29*, 3167–3171.

Scheme 5

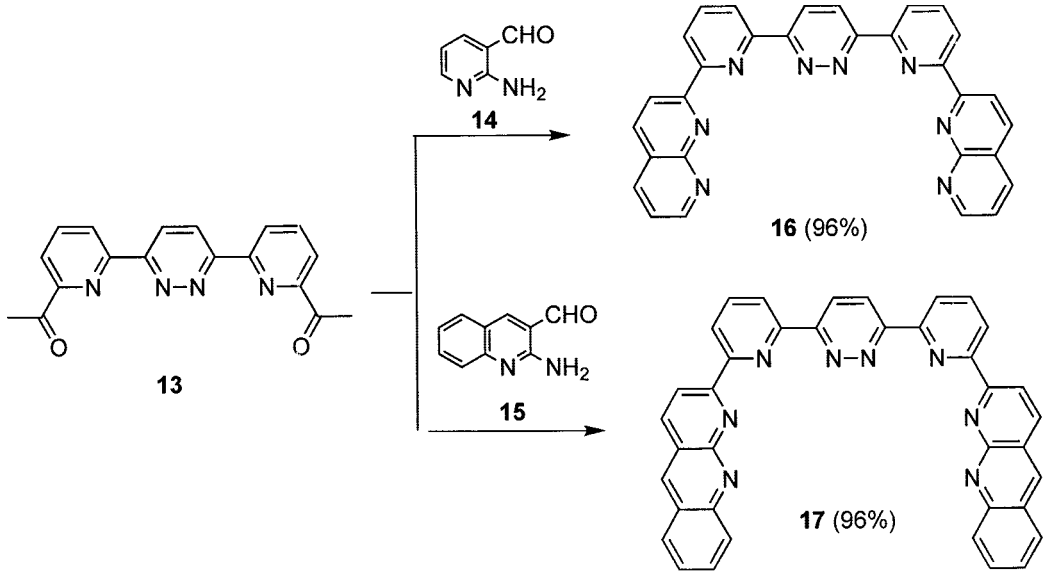

This convergent approach allowed for the variation of the two peripheral azaaromatic binding sites by variation of the aminoaldehyde partner. Thus, the condensation of 2-aminoquinoline-3-carbaldehyde (**15**)[19] afforded the dibenzo derivative of **16** (**17**) in comparably good yield (Scheme 5).

The central linker group on the BL could be varied by using 1,4-dichlorophthalazine (**19**) in the initial coupling reaction with stannane **18**, which is prepared from the ethylenedioxy-protected derivative of 6-bromo-2-acetylpyridine.[20] Deprotection of the intermediate **20** provided the diacetyl derivative **21**, which could then undergo a double Friedländer condensation with either **14** or **15** to afford excellent yields of the BLs **22** and **23**, respectively (Scheme 6).

In a final variation on the BL, we decided to examine a simpler bis-tridentate system **26** involving three, rather than five, azaaromatic rings. This ligand has less conformational freedom than the systems having a 2,6-pyridyl linker and also uses all six of its N lone pair electrons in binding the two Ru centers. The diphenanthrolinylpyridazine **26** was prepared by the Friedländer reaction of 8-aminoquinoline-7-carbaldehyde (**25**)[21] with 3,6-diacetylpyridazine (**24**) as described earlier (Scheme 7).[3]

Conversion of the BLs to their dinuclear Ru(II) complexes involved the self-assembly of eight components: the BL, two Ru ions, four axial pyridine ligands, and a bridging Cl. In earlier work from our group, as well as that of Catalano, this assembly process has not always been straightforward, especially for bis-bidentate ligands. For bis-tridentate BLs, however, additional restrictions (six Ru−N bonds) are placed on the system in the initial coordination of the two metal ions with the BL. Because of the bulk and steric environment of the binding cavity, the likelihood for the formation of $[Ru(BL)_2]$-type complexes is small. Furthermore, in the systems having a pyridazine or phthalazine unit linking the two halves of the BL, there is insufficient space for two pyridines in the remaining equatorial sites, which are instead comfortably spanned by a bridging Cl. This leaves the four axial sites, initially occupied by Cl ions from the $RuCl_3 \cdot 3H_2O$ or $Ru(DMSO)_4Cl_2$ reagent, which are then replaced by the axial pyridines. The complexes are formed in a one-pot reaction, and yields vary in the range of 20–49%. Typically, the complexes are precipitated as their hexafluorophosphate salts and purified by chromatography on alumina. All of the dinuclear complexes prepared in this study are summarized in Chart 1.

Identification of both of the complexes and ligands is readily accomplished by consideration of their NMR spectra. All of the ligands have a C_2 symmetry axis, which reduces the number of signals by half. Additionally, the BLs consist of separate and discrete spin systems involving 2–4 interacting protons. By consideration of chemical shifts, multiplicities, and coupling constants, these signals, which are usually well resolved, can be confidently assigned. In the dinuclear complexes, the axial pyridines are distinct and very characteristic. Because the pyridine is substituted in the 4 position, H2′ and H3′ appear as a pair of doublets in the upfield portion of the aromatic region, with H3′ being at considerably higher field than H2′ which is deshielded by the adjacent N. Each of the two pyridine signals integrates for eight protons, which is 4 times the intensity of each proton from the BL. It appears that, on the NMR time scale, the axial pyridines are freely rotating about the Ru−N bond so that H2′ = H6′ and H3′ = H5′.

A typical ^{1}H NMR spectrum for the complex **30a** in CD_3CN is illustrated in Figure 1, and several features are worthy of note. The proton H1 is held in a very deshielding environment. Feeling effects from the adjacent N1 as well as the Cl and the naphthyridine across the bay region of the complex (see X-ray discussion below), it appears at 10.05 ppm. It is especially interesting that H2, which points away

(19) Godard, A.; Quéguiner, G. *J. Heterocycl. Chem.* **1980**, *17*, 465–473.
(20) Parks, J. E.; Wagner, B. E.; Holm, R. H. *J. Organomet. Chem.* **1973**, *56*, 53–66.
(21) Riesgo, E. C.; Jin, X.; Thummel, R. P. *J. Org. Chem.* **1996**, *61*, 3017–3022.

Scheme 6

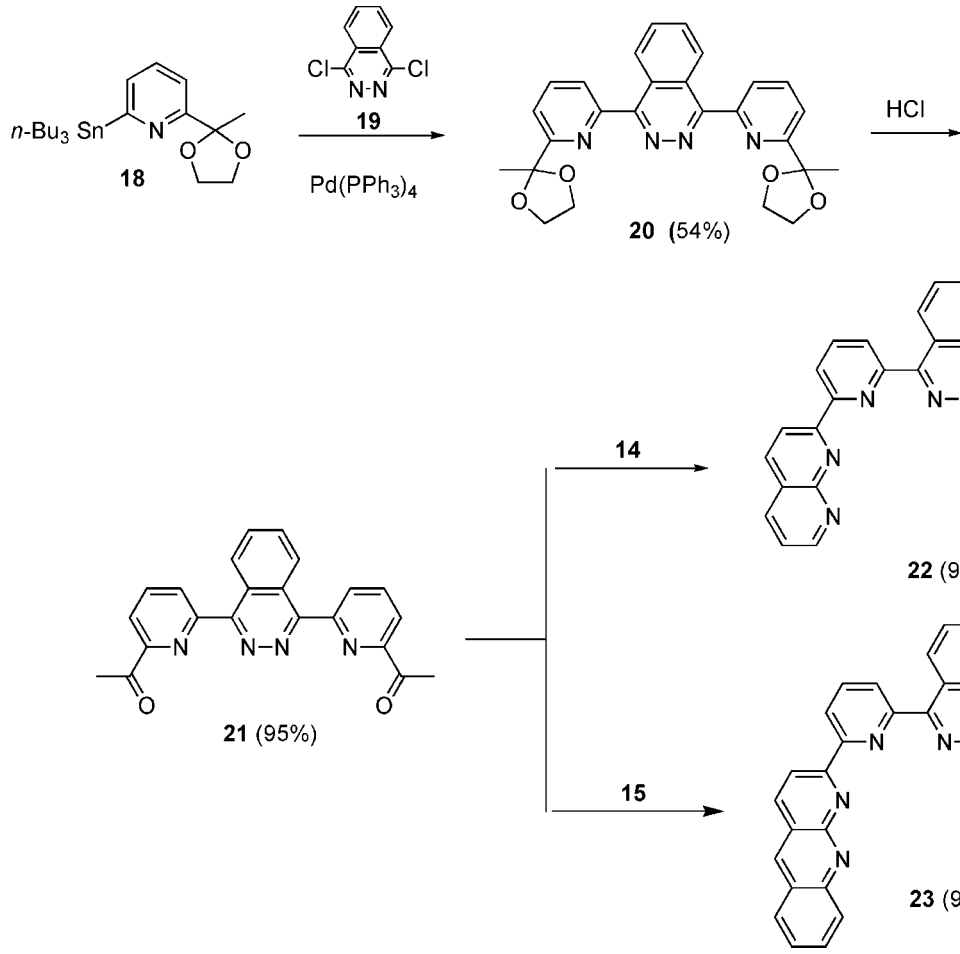

Scheme 7

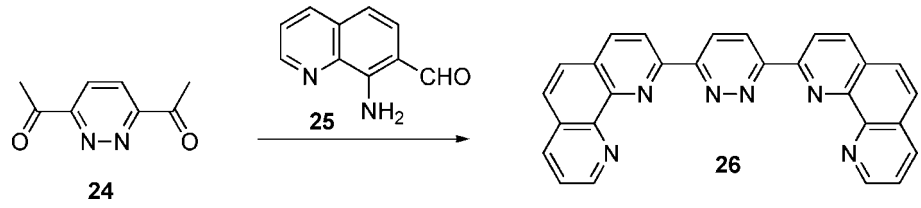

from this deshielding region, is the highest-field signal on the equatorial ligand, appearing at 8.22 ppm. Both H8 and H9 are also held in a congested and strongly deshielded region, appearing at low field, 9.56 and 9.45 ppm, respectively. Protons H5 and H6 similarly occupy a somewhat deshielded region and hence appear downfield from their adjacent protons H4 and H7. In the upfield region of the NMR, one observes a singlet for the 4-substituent when it is methyl, methoxy, *tert*-butyl, and dimethylamino. When 3,5-dimethylpyridine is the axial ligand, the barrier to rotation about the Ru−N bond is sufficiently high that two singlets are observed for the nonequivalent methyl groups.

To further characterize the structure of these dinuclear complexes, we carried out a single-crystal X-ray analysis of **30a**. Figure 2 shows top and side views of the cation $[Ru_2(\mathbf{22})(4\text{-}CH_3\text{-}py)_4Cl]^{3+}$, and Table 1 summarizes some of the pertinent geometric features of the complex. The tridentate binding of the BL to each Ru center is typical of terpyridine-type complexes. The central Ru−N bond is shorter (1.93–1.94 Å) than the outer Ru−N bonds. The Ru is held closer to the interior phthalazine N (2.03–2.04 Å) than it is to the outer naphthyridine N (2.12–2.13 Å), and this disposition may be partly due to the bridging Cl, which completes a five-membered ring including N17 and N26. The Ru−Cl bond, at 2.40 Å, is just slightly shorter than a similar Cl-bridged Ru dimer reported by Catalano having Ru−Cl distances of 2.43 and 2.44 Å.[12a]

Although the BL appears to be relatively planar, there is some dihedral distortion, especially involving the central phthalazine ring. Because of nonbonded interactions between C15−H and C20−H as well as between C23−H and C29−H, the phthalazine twists along the C16−C18 and C25−C28 bonds. Dihedral angles on either side of these bonds average about 15°. Nevertheless, this distortion does not seem to have any serious

Chart 1. Dinuclear Ru(II) Complexes Used as Water Oxidation Catalysts[a]

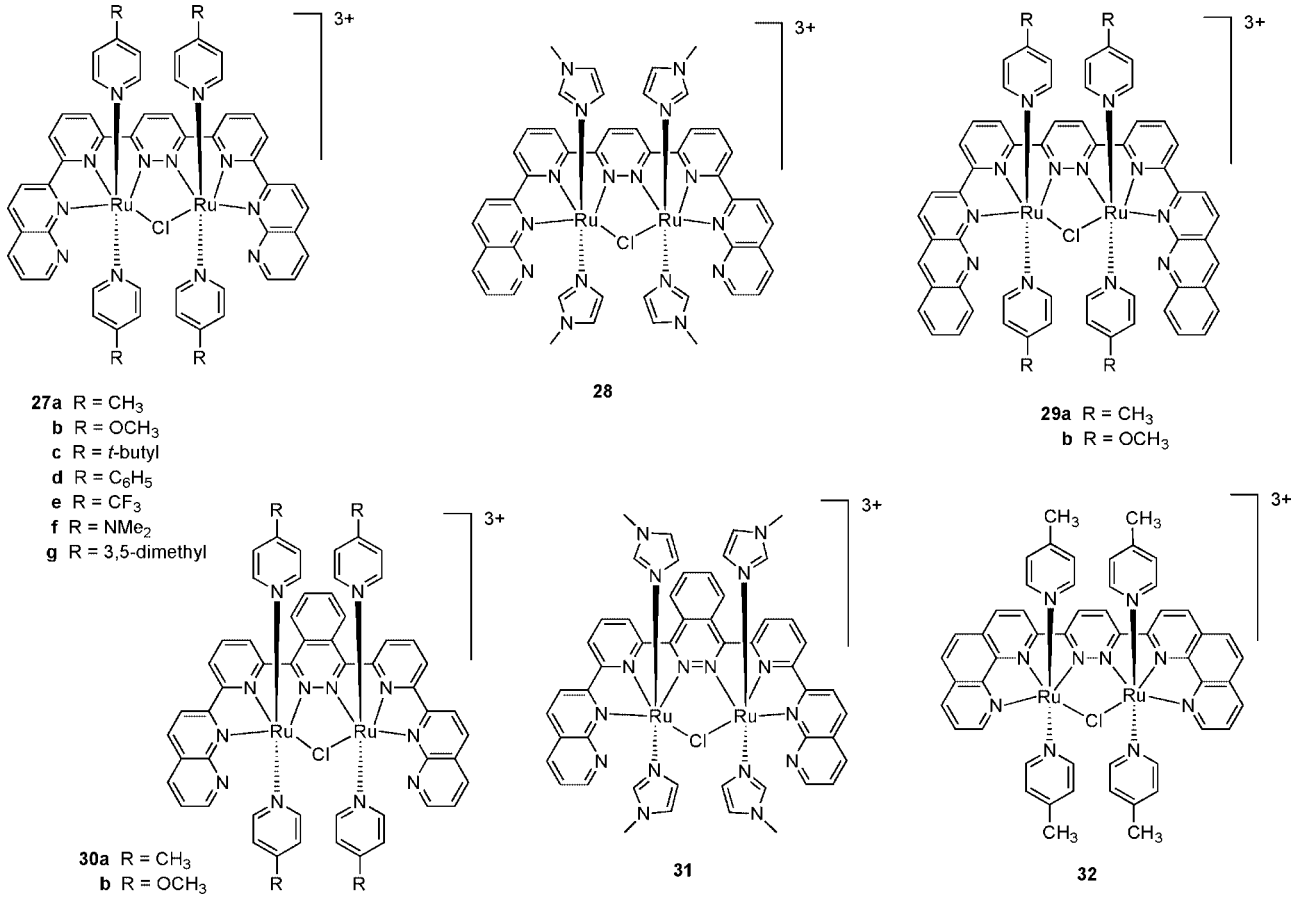

[a] All were prepared as PF_6 salts.

influence on the binding of the metal ions in the cavity of the BL. The N11−Ru1−Cl and N27−Ru2−Cl angles are reasonably linear at about 174–175°.

The most serious distortion caused by the complexation of the two metal centers is a contraction of the interior cavity of the BL. The five separate aromatic rings of the BL are connected by four C−C single bonds, and it is the flexibility associated with these bonds that allows this considerable distortion. Figure 3 illustrates this distortion by showing a superimposition of the BL **22** and its dinuclear complex **30a**. At the mouth of the BL cavity, the N3−N41 distance contracts from an estimated 9.50 Å in the free ligand to 5.17 Å. It is interesting to speculate on the role of the outer noncoordinated pyrido rings of the 1,8-naphthyridine moieties. To some extent, these rings "protect" the Ru−Cl−Ru functionality, which is the likely site of catalytic activity. In a somewhat related study, we have examined other Ru systems having a similar uncoordinated naphthyridyl N, which we hypothesized might act as a photoinitiated internal base for the deprotonation of a metal-bound water molecule.[22]

It is also noteworthy that the four axial pyridine rings lie in approximately parallel planes and the mean distance of 3.66 Å between these planes is within the range for some stabilizing $\pi-\pi$ interaction. Although this arrangement clearly exists in the solid state, the NMR spectra of all of the complexes show only two signals from the 4-substituted pyridines, indicating that rotation around the Ru−N bond is facile in solution.

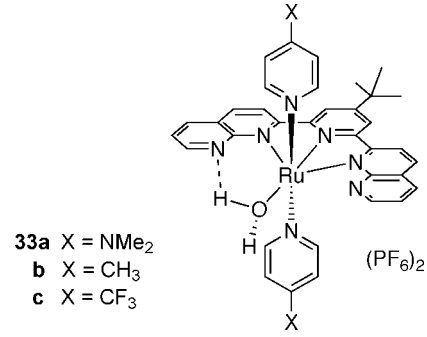

Properties of the Complexes

The electronic absorption spectra of the dinuclear complexes were measured at room temperature in acetone, and these data are recorded in Table 2. The energies and intensities of the electronic transitions are affected by the structures of both the axial and equatorial ligands. In earlier work, we examined the photophysical properties of a tridentate mononuclear analogue of the systems under study here.[4] These complexes **33a**−**c** showed a broad metal-to-

(22) Zong, R.; Naud, F.; Segal, C.; Burke, J.; Wu, F.; Thummel, R. *Inorg. Chem.* **2004**, *43*, 6195–6202.

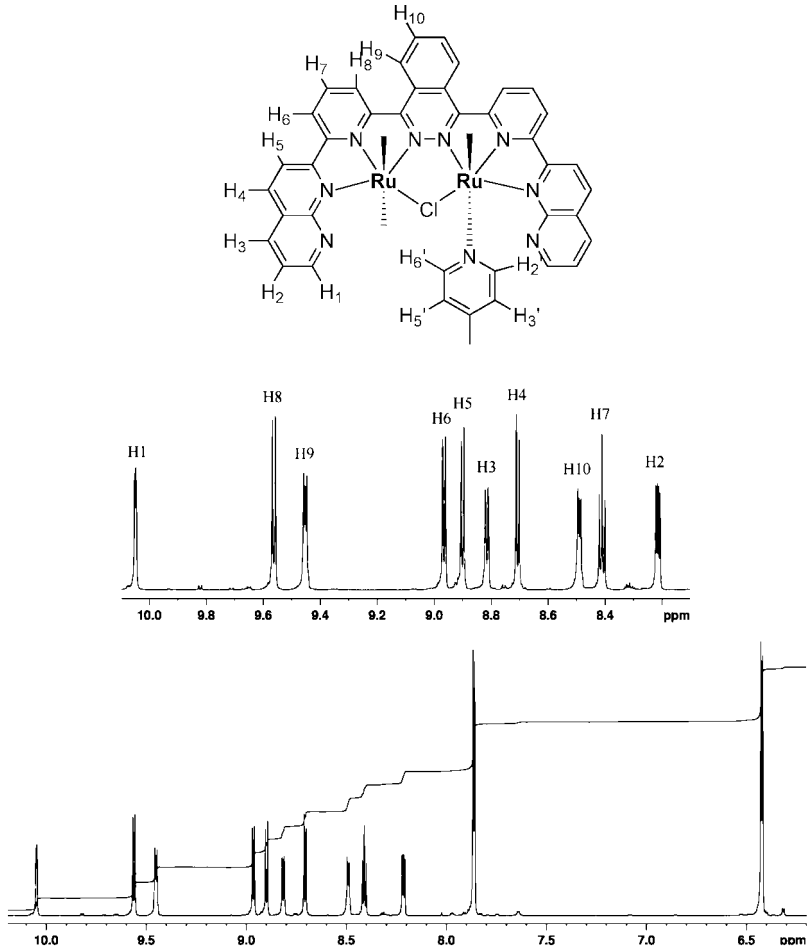

Figure 1. Downfield region of the 800 MHz ^{1}H NMR spectrum of **30a** recorded at 25 °C in CD_3CN.

ligand charge-transfer (MLCT) band spanning about 350 nm whose maxima were very sensitive to the 4-substituent on the two axial pyridine ligands. Although there was a small and consistent variation in the intensities of these bands, their energies showed a shift to lower energy as the 4-substituent became a better donor (NMe_2). Thus, 4-(dimethylamino)pyridine is better able to stabilize the Ru(III) center, which is generated upon photoexcitation.

The series of dinuclear complexes **27a**−**g** show this same dependence such that the system having CF_3-substituted pyridine as an axial ligand absorbs at 571 nm as compared with 577 nm for the mononuclear analogue while the dimethylamino-substituted system absorbs at 685 nm as compared with 669 nm for **33a**. Figure 4 illustrates this situation, with the 4-methyl- and 4-methoxy-substituted axial ligands showing intermediate behavior. Along with variation in the absorption energies, there is a change in the relative importance of the vibrational components of each band much more so than in the mononuclear systems. The relative intensity of the high-energy component at about 490 nm decreases as the pyridine substituent becomes more electron-donating.

Variation in the equatorial ligand also has a pronounced effect on the band shape and energy. Figure 5 illustrates the situation where the axial ligand is kept unchanged as a 4-methylpyridine and the equatorial ligand is modified. Changing the central linker from pyridazine to phthalazine increases the high-energy component of the absorption at 550 nm at the expense of the lower energy bands at 646 and 721 nm. When the peripheral ligating moiety is changed from 1,8-naphthyridyl to benzo-1,8-naphthyridyl, the π^* energy of the acceptor orbital is lowered and the band shifts to 673 nm. The complex **32** shows an MLCT centered at 494 nm, similar to **27**−**31**. Because of the fact that the BL in **32** contains only three azaaromatic rings as compared to five in the other systems, this complex enjoys less conformational mobility, and the resulting rigidification is reflected by the more pronounced vibrational structure observed in its absorption band.

The half-wave potentials for the dinuclear complexes were measured in acetonitrile, and the data are recorded in Table 2. The oxidation of such Ru(II) complexes involves the removal of an electron from the highest occupied molecular orbital, which is usually a metal-based d orbital, while reduction involves the addition of an electron to the lowest unoccupied molecular orbital, which is generally a π^* orbital on the most electronegative ligand.[23] Initially, it is constructive to consider the series of complexes **27a**−**g** and **28**, in which the equatorial ligand remains constant (**16**). The oxidation potential is sensitive to the 4-substituent on the axial pyridine ligands. When this group is the strongly electron-withdrawing CF_3, the Ru(III) state becomes destabilized and the removal of an electron requires a higher

(23) Kalyanasundaram, K. *Photochemistry of Polypyridine and Porphyrin Complexes*; Academic Press: San Diego, 1992.

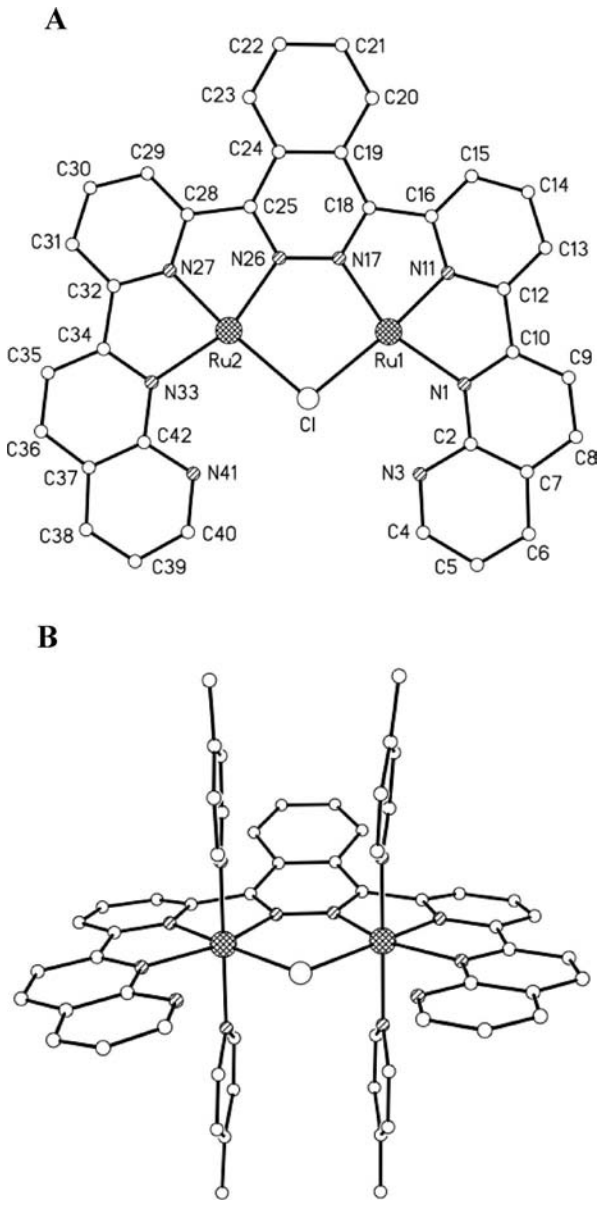

Figure 2. Top (A) and side (B) views of the cation of **30a** with atomic numbering scheme. For clarity, the axial ligands have been omitted from view A and the hydrogens from both views.

Table 1. Selected Geometric Data for Complex **30a**

Bond Lengths (Å)			
Ru1−N1	2.116(5)	Ru2−N33	2.133(5)
Ru1−N11	1.934(5)	Ru2−N27	1.941(5)
Ru1−N17	2.037(5)	Ru2−N26	2.032(5)
Ru1−N43	2.096(5)	Ru2−N57	2.097(5)
Ru1−N50	2.092(5)	Ru2−N64	2.107(5)
Ru1−C1	2.4057(17)	Ru2−C1	2.3976(16)
Bond Angles (deg)			
N11−Ru1−C1	174.15(16)	N27−Ru2−C1	174.93(17)
Ru1−C1−Ru2	99.67(6)		
Dihedral Angles (deg)			
C16−C18−C19−C20	−10.9(11)	C16−C18−C19−C20	11.0(11)
C15−C16−C18−C19	−18.2(11)	C15−C16−C18−C19	18.8(11)
N11−C16−C18−N17	−11.0(8)	N11−C16−C18−N17	11.8(8)
C9−C10−C12−C13	5.0(11)	C9−C10−C12−C13	−1.5(12)
N1−C10−C12−N11	3.2(8)	N1−C10−C12−N11	−0.6(9)

potential (1.47 V). However, when the 4-substituent is an electron-donating dimethylamino group, the Ru(III) state is stabilized and oxidation occurs at a lower potential (0.92 V). The alkyl- and phenyl-substituted systems are very similar at 1.21–1.25 V, while methoxy- and 3,5-dimethyl-substituted systems are slightly lower at 1.13 V. When the electron-rich imidazole is used as an axial ligand (**28**), it behaves much like dimethylamino (0.93 V). In the complexes **29a**,**b**, the equatorial ligand **17** is just a dibenzo-fused analogue of **16** and this perturbation has only a small effect on the oxidation potential. When the equatorial ligand is perturbed instead by benzo fusion to the central pyridazine ring, again the effect observed for **30a**,**b** is small. However, for **31**, with an imidazole axial ligand, oxidation becomes easier (0.90 V) and comparable to the dimethylamino system.

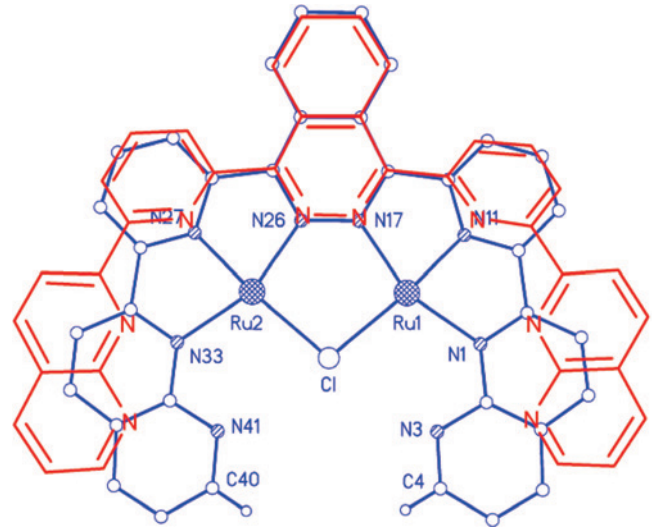

Figure 3. Overlay of the optimized geometry (AM-1) for ligand **22** (red) and the equatorial plane of the complex **30a** (blue) as determined by X-ray crystallography.

For each of these systems, the two Ru(II) centers are strongly coupled and thus a second oxidation wave ($Ru^{II,III} \rightarrow Ru^{III,III}$) is observed at 0.24–0.55 V higher potential. If the two Ru(II) centers were noninteracting, they would both be expected to oxidize at the same potential. The second oxidation wave for **27e** is outside the observation window for our solvent system. The complex **32** exhibits two oxidation waves that are slightly more positive than the other three systems having axial 4-methypyridines (**27a**, **29a**, and **30a**).

The reductions are similarly well-behaved. Because this process is ligand-based, **27a**−**g** and **28**, having the same equatorial ligand, are comparable, with the exception of the three systems having strong donor or acceptor groups as axial ligands. Thus, we observe first reductions in the range of –0.54 to –0.85 V and second reductions at –0.94 to –1.16 V. In many cases, third and even fourth reductions can be detected. Benzo fusion on the naphthyridyl rings of the BL **16** increases delocalization and leads to a slight increase of the first reduction (−0.62 V) and a significant increase of the second reduction (−0.74 V).[24] Benzo fusion on the central pyridazine ring leads to an even more impressive increase in the reduction potential to –0.42 V for **30a**,**b**. As

(24) Thummel, R. P.; Decloitre, Y. *Inorg. Chim. Acta* **1987**, *128*, 245–249.

Table 2. Electronic Absorption[a] and CV[b] Data for Dinuclear Ru(II) Complexes

complex	λ_{max}, nm (ϵ, M^{-1} cm^{-1})	$E_{1/2}^{ox.}$ (ΔE)	$E_{1/2}^{red.}$ (ΔE)
27a	338 (45 480), 505 (7280), 613 (8550)	1.25 (99), 1.66 (110)	−0.65 (72), –1.02 (76), –1.24 (82), –1.73 (81)
27b	324 (34 708), 339 (43 322), 509 (5278), 634 (8666)	1.13 (99), 1.51 (119)	−0.71 (89), –1.07 (74)
27c	340 (47 734), 505 (7730), 619 (9558)	1.21 (99), 1.65 (121)	−0.68 (100), –1.05 (84), –1.28 (86)
27d	340 (46 472), 502 (8062), 610 (9274)	1.24 (87), 1.64 (97)	−0.65 (66), –1.02 (68), –1.22 (79)
27e	340 (43 240), 380 (18 950), 484 (10 950), 571 (9830)	1.47 (127)	−0.54 (95), –0.94 (73)
27f	338 (44 970), 503 (3984), 525 (3896), 685 (5500)	0.92 (85), 1.16 (118)	−0.74 (77), –1.07 (86), –1.33 (99)
27g	340 (44 774), 502 (8550), 610 (9940)	1.13 (87), 1.68 (99)	−0.69 (129), –1.04 (95), –1.10 (313)
28	324 (29 014), 337 (36 372), 527 (4530), 667 (7804)	0.93 (99), 1.23 (98)	−0.85 (68), –1.16 (84), –1.41 (123)
29a	364 (42 542), 669 (7498)	1.12 (84), 1.62 (94)	−0.62 (60), –0.74 (69), –1.09 (216)
29b	332 (37 568), 363 (40 204), 522 (4842), 673 (8150)	1.16 (77), 1.52 (92)	−0.62 (63), –0.74 (76), –1.10 (218)
30a	343 (49 322), 445 (6026), 550 (10 992), 646 (6548), 721 (4980)	1.20 (97), 1.56 (107)	−0.42 (94), –0.92 (89), –1.30 (112), –1.69 (213)
30b	324 (34 666), 338 (40 246), 551 (7920), 649 (5416), sh, 750 (2316)	1.12 (82), 1.43 (97)	−0.42 (100), –0.91 (87), –1.43 (130), –1.71 (49)
31	324 (28 808), 338 (34 810), 576 (4674), 696 (3960), sh, 770 (2278)	0.90 (79), 1.19 (89)	−0.59 (79), –1.10 (80), –1.43 (130), –1.71 (49)
32	348 (30 466), 457 (7338), 494 (9690), 528 (8304), 565 (6816), 669 (2098)	1.32 (83), 1.75 (109)	−0.54 (75), –0.94 (74), –1.75 (117)

[a] Measured in acetone (5.0×10^{-5} M). [b] Measured with a glassy carbon electrode at 100 mV/s in CH_3CN containing 0.1 M $N(n\text{-}Bu)_4PF_6$ and reported in volts relative to SCE; $E_{1/2} = (E_{pa} + E_{pc})/2$ in volts and $\Delta E = (E_{pa} - E_{pc})$ in millivolts.

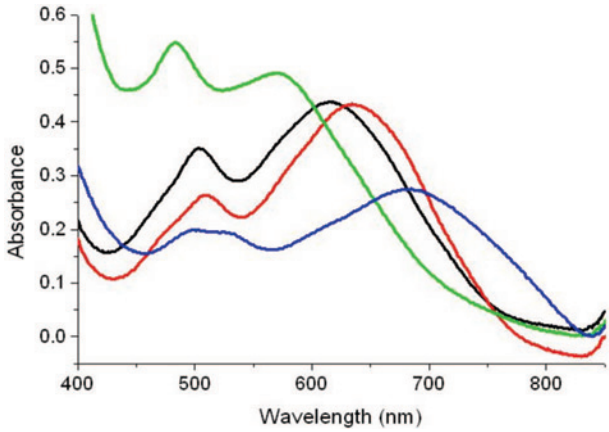

Figure 4. Electronic absorption spectra recorded in acetone (5×10^{-5} M): **27a** (black), **27b** (red), **27e** (green), **27f** (blue).

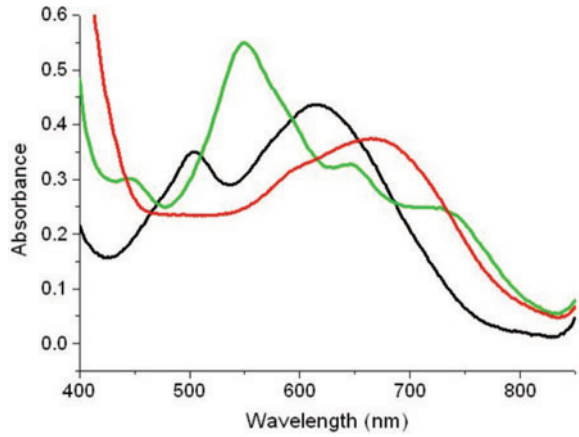

Figure 5. Electronic absorption spectra recorded in acetone (5×10^{-5} M): **27a** (black), **29a** (red), **30a** (green).

in the case of **28**, the donating effect of the axial imidazole ligand causes a significant decrease in the reduction potential of **31**. Although the BL in **32** differs somewhat in structure from the other systems, its reduction potentials are not significantly different.

Catalytic Activity

The first dinuclear catalyst that we prepared in this study was **27a**, and once its structure was verified, it was tested for catalytic activity by adding a minute amount (<1 mg) to a solution of excess ceric ammonium nitrate in aqueous trifluoromethanesulfonic acid adjusted to pH = 1. Copius bubbles were observed to form almost immediately and, after some time, the yellow color of the Ce(IV) faded markedly. Since then, we have used three methods to monitor oxygen evolution with some variation in the results. At first, we used a YSI electrochemical oxygen probe located in the headspace above the reaction mixture.[25] We found that this probe was sensitive to both temperature and pressure. Using a thermostatted reaction cell solved the temperature problem, and we calibrated the electrode over the useful pressure range of generated oxygen. The initial performance was good, but eventually the silver electrode broke down under the strongly oxidizing and acidic atmosphere (pH = 1).

Gas chromatography (GC) analysis was simple and more reliable.[26] The reaction could be run in a closed vessel (septum cap) and the head gas sampled at regular intervals. Using a 5A molecular sieve column, we were able to readily separate oxygen and nitrogen, and using argon as a carrier gas would even allow for the detection of hydrogen if it was present. For simplicity, we use air in the headspace and thus nitrogen serves as an internal standard. The only drawback to this method is that it is tedious to record time-dependent (kinetic) data in this fashion. To solve this problem, we used an optical oxygen sensor, which relied on fluorescence quenching by oxygen to monitor its concentration. This method, checked routinely against GC, proved to be both rugged and reliable.

For all of the reported dinuclear complexes, we measured the catalyst stability or turnover number (TN) by GC, with a typical end point coming after 48 h. We also measured oxygen evolution versus time with the optical probe and thus were able to determine the rates of oxygen production. All these data are collected in Table 3. It should be noted that all of the TN data were measured by GC analysis, and these more reliable numbers differ somewhat from those which

(25) Yamada, H.; Siems, W. F.; Koike, T.; Hurst, J. K. *J. Am. Chem. Soc.* **2004**, *126*, 9786–9795.
(26) Hara, M.; Waraksa, C. C.; Lean, J. T.; Lewis, B. A.; Mallouk, T. E. *J. Phys. Chem. A* **2000**, *104*, 5275–5280.

Table 3. TN and Rate Data for Water Oxidation

complex	TN	rate[a] (μmol/min)	relative rate	complex	TN	rate[a] (μmol/min)	relative rate
27a	538	0.556	31	**28**	0[b]	0[b]	
27b	689	0.924	51	**29a**	459	0.488	27
27c	561	0.586	33	**29b**	601	0.837	47
27d	80	0.018	1	**30a**	572	0.614	34
27e	116	0.062	3	**30b**	610	0.863	48
27f	112	0.323	18	**31**	0[b]	0[b]	
27g	443	0.582	32	**32**	597	0.480	27

[a] A second-order polynomial was used to fit the generated oxygen vs time curves (Figure 6) in the period of 0–60 min; rate = slope of the curve at 30 min. [b] Too low to measure under general reaction conditions.

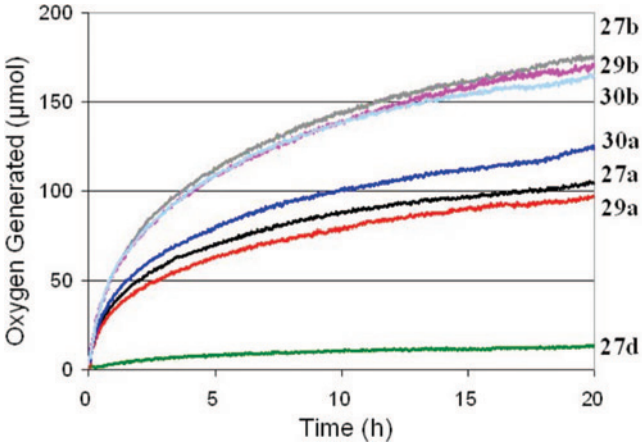

Figure 6. Kinetic plots of oxygen evolution vs time. The catalyst structure numbers are given along the right vertical axis.

we reported earlier for **27a**,**e**,**f** as measured with the YSI electrochemical probe.[25]

The catalyst that generates oxygen at the fastest rate is **27b**, while the slowest measurable system is **27d**. Both **28** and **31**, having *N*-methylimidazole at the axial sites, are too slow to measure and essentially generate no oxygen. It should be remembered that at pH = 1 *N*-methylimidazole is most likely protonated. Figure 6 illustrates the kinetic plots for seven of the catalyst systems, and several general features are evident. The systems having 4-methoxypyridine as the axial ligand appear to be the most active (**27b**, **29b**, and **30b**), while those with 4-methylpyridine (**27a**, **29a**, **30a**, and **32**) are somewhat less reactive. The slowest system **27d** shows the lowest slope.

The TNs correlate reasonably well with the rates, with the fastest system having the highest TN (**27b**). The imidazole systems **28** and **31** do not generate any perceptible oxygen under the given reaction conditions. Figure 7 shows a plot of TN vs relative rate. The point that is farthest out of line is that for **27f** and, here again, one should remember that the dimethylamino substituent on the axial pyridine is probably protonated at pH = 1.

For catalyst **27a**, which is one of the more active systems, we also measured the rate of oxygen evolution as a function of the catalyst concentration. Figure 8 shows the results for water decomposition catalyzed by 0.05, 0.1, 0.15, and 0.2 μmol of **27a**. The amount of oxygen generated shows a linear progression indicating that the reaction is first-order in catalyst. This result is consistent with a pathway that would involve the cooperative interaction of the two Ru centers of

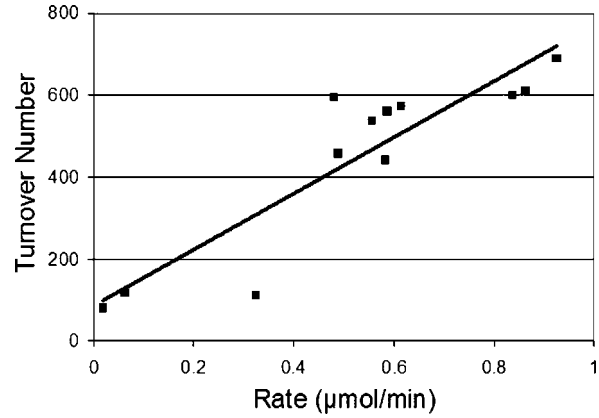

Figure 7. Comparison of TNs and the rates of oxygen evolution for all 12 active catalysts.

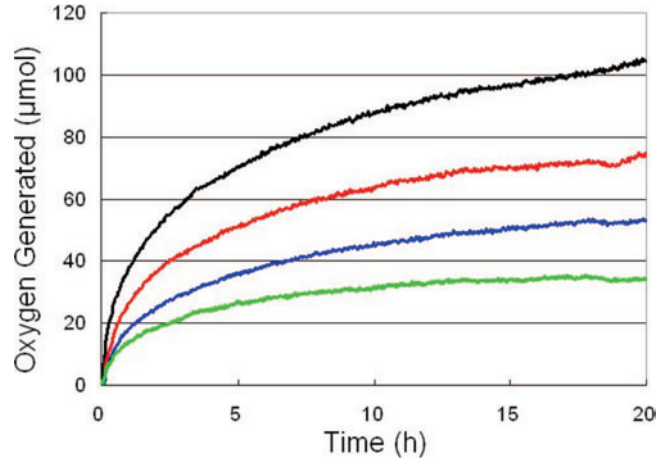

Figure 8. Kinetic plot of oxygen evolution vs time at various concentrations of catalyst **27a**: 0.5×10^{-4} mmol (green), 1.0×10^{-4} mmol (blue), 1.5×10^{-4} mmol (red), 2.0×10^{-4} mmol (black).

a single catalyst molecule. However, we have also examined analogous mononuclear catalysts that show a similar first-order dependence on the catalyst concentration. These observations raise interesting questions that will be considered in future work.

Closing Remarks

A series of 14 symmetrical dinuclear Ru(II) complexes have been prepared involving four closely related polydentate BLs. These complexes self-assemble in a one-pot reaction that incorporates both Ru(II) centers as well as a bridging Cl ion and four monodentate axial pyridines or *N*-methylimidazoles to complete the coordination sphere of the metals. All of the complexes are readily characterized in solution by ^{1}H NMR spectroscopy, and they exhibit photophysical and electrochemical properties that are consistent with electronegativity and delocalization effects due to the ligands. In the presence of a sacrificial chemical oxidant [Ce(IV)], all but two of the complexes catalyze the decomposition of water to molecular oxygen. The TNs and rates of oxygen generation correlate reasonably well so that the more active catalysts also show greater stability.

In future work, we will continue to study these dinuclear systems, particularly from an electrochemical perspective,[27] to try to understand more about how they function. We will also examine in detail the analogous chemistry of their mononuclear counterparts. Most importantly, we will use synthesis to prepare more active catalysts by incorporating features that have been shown to lead to more efficient oxygen generation. A truly practical water oxidation catalyst must function much better than the ones described in this work. Also we will need to consider the reduction side of the problem and the harvesting of hydrogen from the protons liberated in the oxidation reaction. Finally, we must address the issue of photoreactivity and find a way to drive these reactions with light. The challenge is a considerable one, but it is well suited to modern chemistry.[28] The payoff of clean-burning hydrogen derived from the interaction of sunlight with water will be a huge contribution to the betterment of mankind.

Experimental Section

NMR spectra were recorded on a General Electric QE-300 or a Bruker 800 MHz NMR spectrometer. Chemical shifts are reported in parts per million downfield from Me_4Si. Electronic absorption spectra were recorded with a Perkin-Elmer Lambda 3B spectrophotometer. All spectra were corrected for the background spectrum of the solvent. Cyclic voltammetric (CV) measurements were carried out with a BAS Epsilon electroanalytical system using a one-compartment cell equipped with a glassy carbon working electrode, a saturated calomel reference electrode (SCE), and a Pt wire as the auxiliary electrode. An acetonitrile solution of $(n\text{-Bu})_4N(PF_6)$ (0.1 M) in a tube with a porous glass frit on one end was used between the SCE electrode and the sample solution. IR spectra were taken on a Thermo Nicolet AVATAR 370 Fourier transform IR spectrometer. Elemental analyses were performed by Quantitative Technologies Inc., Whitehouse, NJ. Melting points were obtained on a Thomas-Hoover capillary melting point apparatus and are uncorrected. Mass spectra were obtained on a Thermo-Finnigan LCQ Deca XP Plus spectrometer. A modified household microwave oven (Samsung MW2000U, 950 W, 60 Hz) was used in the preparation of some complexes.[29]

$[Pd(PPh_3)_4]$,[30] $Ru(DMSO)_4Cl_2$,[31] 2-aminonicotinaldehyde,[32] 2-aminoquinoline-3-carbaldehyde (**15**),[18] 3,6-bis(6′-acetylpyrid-2′-yl)-pyridazine (**13**),[3] 3,6-bis[6′-(1″,8″-naphthyrid-2″-yl)pyrid-2′-yl]-pyridazine (**16**),[3] 6-(1′,1′-ethylenedioxyethyl)-2-(tri*n*-butylstannyl)-pyridine (**18**),[3] 3,6-bis(1′,10′-phenanthrolin-2′-yl)pyridazine (**26**),[3] and complexes **27a**,**e**,**f**[4] were prepared according to published procedures. All other chemicals are commercially available, and all solvents are reagent grade.

The rate of oxygen evolution was measured with an Ocean Optics (FOXY-OR125-G) oxygen sensor interfaced to a PC and a 10 mL round-bottomed flask with a threaded side arm for introduction of the sensor probe. This probe was calibrated prior to use by GC as described below. The flask was charged with $Ce(NH_4)_2(NO_3)_6$ (550 mg, 1 mmol), and 3 mL of CF_3SO_3H(aq) (adjusted to pH = 1) was added to give a homogeneous solution, which was stirred at 20 °C. The complex (2.0×10^{-4} mmol) was dissolved in CH_3CN (50 μL) and then injected into the solution through a septum cap. The generated oxygen was measured, and readings were recorded every 2 min for 20 h.

TNs were measured in the following manner. To a 10 mL one-neck, round-bottomed flask were added $Ce(NH_4)_2(NO_3)_6$ (550 mg, 1 mmol) and 3 mL of CF_3SO_3H(aq) (adjusted to pH = 1), and the mixture was magnetically stirred to give a homogeneous solution. The complex (2.0×10^{-4} mmol) dissolved in CH_3CN (50 μL) was injected into the solution through a rubber septum, and the mixture was stirred at room temperature for 48 h. The oxygen content in the headspace of the flask was measured using a Gow-Mac series 400 thermal conductivity GC with a 6 ft × $^1/_8$ in. 5A molecular sieve column operating at 70 °C and 20 mL/min of Ar.

3,6-Bis[6′-(benzo[*b*]-1″,8″-naphthyrid-2″-yl)pyrid-2′-yl]pyridazine (17). A mixture of **13** (110 mg, 0.345 mmol), **15** (130 mg, 0.76 mmol), and saturated ethanolic KOH (2 mL) in absolute ethanol (50 mL) was refluxed for 24 h. The reaction mixture was concentrated, and the residue was washed with water (2 × 3 mL), EtOH (3 mL), and ether (2 × 3 mL) to afford a dark-gray solid (170 mg, 84%). Mp: >270 °C. ^{1}H NMR ($CDCl_3$ + CD_3OD): δ 9.13 (d, 2H, J = 7.5 Hz), 9.02 (s, 2H), 8.94 (m, 4H), 8.59 (d, 2H, J = 9.1 Hz), 8.41 (d, 2H, J = 8.7 Hz), 8.19 (t, 2H, J = 8.1 Hz), 8.09 (d, 2H, J = 9.1 Hz), 7.89 (t, 2H, J = 4.5 Hz), 7.64 (m, 2H), 7.32 (m, 2H). ^{13}C NMR could not be obtained because of poor solubility. Anal. Calcd for $C_{38}H_{22}N_8 \cdot H_2O$: C, 75.00; H, 3.95; N, 18.42. Found: C, 74.99; H, 3.94; N, 18.23.

1,4-Bis[6′-(1″,1″-ethylenedioxyethyl)pyrid-2′-yl]phthalazine (20). A mixture of **18** (1.14 g, 2.5 mmol), **19** (219 mg, 1.1 mmol), and $Pd(PPh_3)_4$ (110 mg, 0.095 mmol) in dimethoxyethane (20 mL) was heated for 1 week at 80 °C under argon. A dark-red solution was obtained. The solvent was evaporated, and the residue was purified by chromatography on alumina, eluting with hexane/CH_2Cl_2 (1:1) and hexane/EtOAc (1:1) to afford a colorless solid (270 mg, 54%). Mp: 161–163 °C. ^{1}H NMR ($CDCl_3$): δ 8.89 (dd, 2H, J = 6.9 and 3.3 Hz), 8.21 (dd, 2H, J = 7.8 and 1.5 Hz), 7.96 (t, 2H, J = 7.5 Hz), 7.89 (dd, 2H, J = 6.0 and 3.3 Hz), 7.73 (dd, 2H, J = 7.8 and 1.2 Hz), 4.14 (m, 4H), 3.99 (m, 4H), 1.87 (s, 6H).

1,4-Bis(6′-acetylpyrid-2′-yl)phthalazine (21). A mixture of **20** (260 mg, 0.57 mmol) and HCl (2.0 M, 3 mL) in acetone (21.0 mL) was stirred for 40 h at room temperature. The mixture was concentrated to 2 mL and extracted with CH_2Cl_2 (2 × 15 mL). The combined organic phase was washed with water and dried over $MgSO_4$, and the solvent was evaporated to afford the crude product, which was washed with ether (10 mL) to afford a white solid (200 mg, 95%). Mp: 245–246 °C. ^{1}H NMR ($CDCl_3$): δ 8.99 (dd, 2H, J = 6.0 and 3.6 Hz), 8.55 (dd, 2H, J = 7.8 and 1.2 Hz), 8.25 (dd, 2H, J = 7.8 and 1.2 Hz), 8.15 (t, 2H, J = 7.8 Hz), 8.01 (dd, 2H, J = 7.2 and 3.3 Hz), 2.77 (s, 6H). ^{13}C NMR ($CDCl_3$): δ 199.6, 156.2, 155.0, 152.5, 138.3, 132.4, 129.1, 126.9, 126.2, 121.9, 25.9.

1,4-Bis[6′-(1″,8″-naphthyrid-2″-yl)pyrid-2′-yl]phthalazine (22). A mixture of **21** (165 mg, 0.45 mmol), 2-aminonicotinaldehyde (137 mg, 1.13 mmol), and saturated ethanolic KOH (1.0 mL) in absolute ethanol (40 mL) was refluxed for 24 h. The reaction mixture was concentrated, and the residue was washed with water (2 × 3 mL), EtOH (3 mL), and ether (2 × 3 mL) to afford an off-white solid (220 mg, 91%). Mp: >270 °C. ^{1}H NMR ($CDCl_3$ + CD_3OD): δ 9.06 (dd, 2H, J = 4.2 and 1.5 Hz), 8.90 (dd, 2H, J = 9.3 and 1.5 Hz), 8.73 (m, 4H), 8.34 (m, 4H), 8.19 (m, 4H), 7.91

(27) A collaboration has been initiated with Etsuko Fujita at Brookhaven National Laboratories to study the electrochemical properties of our catalysts.
(28) (a) Eisenberg, R.; Nocera, D. G. *Inorg. Chem.* **2005**, *44*, 6799–6801, and following articles. (b) BaumR. M. *Chem. Eng. News* **2005**, *5* (Oct 17).
(29) (a) Matsumura-Inoue, T.; Tanabe, M.; Minami, T.; Ohashi, T. *Chem. Lett.* **1994**, 2443. (b) Arai, T.; Matsumura, T.; Oka, T. *Kagaku To Kyoiku* **1993**, *41*, 278.
(30) Four, P.; Guibe, F. *J. Org. Chem.* **1981**, *46*, 4439–4445.
(31) Duliere, E.; Devillers, M.; Marchand-Brynaert, J. *Organometallics* **2003**, *22*, 804–811.
(32) Majewicz, T. G.; Caluwe, P. *J. Org. Chem.* **1974**, *39*, 720–721.

(dd, 2H, J = 6.9 and 3.6 Hz), 7.56 (dd, 2H, J = 8.4 and 4.2 Hz). ^{13}C NMR ($CDCl_3$ + CD_3OD): δ 158.9, 157.2, 155.3, 154.8, 154.4, 153.6, 138.6, 138.1, 137.4, 132.5, 127.1, 126.5, 126.3, 123.1, 122.7, 122.4, 120.1.

1,4-Bis[6′-(benzo[*b*]-1″,8″-naphthyrid-2″-yl)pyrid-2′-yl]phthalazine (23). A mixture of **21** (122 mg, 0.33 mmol), **15** (125 mg, 0.73 mmol), and saturated ethanolic KOH (1.0 mL) in absolute ethanol (40 mL) was treated as described for **22** to afford a dark-yellow solid (203 mg, 96%). Mp: >270 °C. ^{1}H NMR ($CDCl_3$ + CD_3OD): δ 9.05 (d, 2H, J = 7.2 Hz), 8.84 (s, 2H), 8.80 (dd, 2H, J = 5.4 and 3.3 Hz), 8.68 (d, 2H, J = 8.4 Hz), 8.19 (m, 6H), 7.99 (d, 2H, J = 7.8 Hz), 7.93 (m, 2H), 7.79 (t, 2H, J = 7.2 Hz), 7.53 (t, 2H, J = 7.5 Hz). ^{13}C NMR could not be obtained because of poor solubility. Anal. Calcd for $C_{42}H_{24}N_8 \cdot 2H_2O$: C, 74.48; H, 4.14; N, 16.56. Found: C, 73.98; H, 4.06; N, 16.33.

***trans*,*trans*-[Ru$_2$(16)(4-CH$_3$O-py)$_4$Cl](PF$_6$)$_3$ (27b).** A mixture of **16** (31.4 mg, 0.064 mmol) and [Ru(DMSO)$_4$Cl$_2$] (73.0 mg, 0.15 mmol) in EtOH (40 mL) and CH_2Cl_2 (2 mL) was refluxed for 8 h, producing a dark solution. Water (5 mL) and 4-methoxypyridine (0.3 mL, 2.96 mmol) were added and the mixture was refluxed overnight. Et_3N (0.2 mL) and LiCl (10 mg) were then introduced, reflux was continued an additional 24 h, and the solution was concentrated to about 5 mL. Addition of NH_4PF_6 (62 mg, 0.38 mmol) produced a precipitate which was purified by chromatography on alumina, eluting first with hexanes−acetone (1:1) to remove the impurities. The complex was recovered by eluting with acetone−CH_3CN-saturated aqueous KPF_6 (1:1:0.05) to afford **27b** (45 mg, 43%). Mp: >300 °C. ^{1}H NMR (acetone-d_6): δ 10.01 (dd, 2H, J = 4.5 and 2.4 Hz), 9.36 (s, 2H), 9.16 (d, 2H, J = 7.5 Hz), 8.93 (m, 4H), 8.83 (dd, 2H, J = 8.4 and 2.1 Hz), 8.72 (d, 2H, J = 8.4 Hz), 8.36 (t, 2H, J = 8.1 Hz), 8.22 (dd, 2H, J = 8.1 and 4.5 Hz), 7.79 (dd, 8H, J = 5.7 and 1.2 Hz), 6.23 (dd, 8H, J = 5.7 and 1.5 Hz), 3.53 (s, 12H). Anal. Calcd for $C_{54}H_{46}ClF_{18}N_{12}O_4P_3Ru_2$: C, 40.55; H, 2.90; N, 10.51. Found: C, 40.77; H, 2.70; N, 10.12.

***trans*,*trans*-[Ru$_2$(16)(4-*t*-Bu-py)$_4$Cl](PF$_6$)$_3$ (27c).** The same procedure as that described for **27b** was followed, using **16** (31.4 mg, 0.064 mmol), [Ru(DMSO)$_4$Cl$_2$] (73.0 mg, 0.15 mmol), and 4-*tert*-butylpyridine (0.3 mL, 3.33 mmol) to afford **27c** (20 mg, 20%). Mp: >300 °C. ^{1}H NMR (acetone-d_6): δ 10.05 (dd, 2H, J = 4.5 and 2.4 Hz), 9.41 (s, 2H), 9.20 (d, 2H, J = 7.5 Hz), 8.86 (m, 4H), 8.81 (dd, 2H, J = 8.4 and 1.2 Hz), 8.58 (d, 2H, J = 9.0 Hz), 8.38 (t, 2H, J = 8.7 Hz), 8.23 (dd, 2H, J = 8.7 and 4.5 Hz), 8.03 (dd, 8H, J = 5.7 and 0.6 Hz), 6.63 (dd, 8H, J = 5.7 and 1.8 Hz), 0.76 (s, 36H). Anal. Calcd for $C_{66}H_{70}N_{12}ClP_3F_{18}Ru_2 \cdot 2C_3H_6O$: C, 47.48; H, 4.51; N, 9.23. Found: C, 47.68; H, 4.58; N, 9.09.

***trans*,*trans*-[Ru$_2$(16)(4-Ph-py)$_4$Cl](PF$_6$)$_3$ (27d).** The same procedure as that described for **27b** was followed, using **16** (31.4 mg, 0.064 mmol),[Ru(DMSO)$_4$Cl$_2$] (73.0 mg, 0.15 mmol), and 4-phenylpyridine (0.25 g, 1.6 mmol) to afford **27d** (31 mg, 27%). Mp: >300 °C. ^{1}H NMR (acetone-d_6): δ 10.08 (dd, 2H, J = 3.9 and 1.2 Hz), 9.45 (s, 2H), 9.22 (d, 2H, J = 8.1 Hz), 8.86 (t, 2H, J = 7.8 Hz), 8.79 (dd, 2H, J = 8.4 and 2.4 Hz), 8.62 (d, 2H, J = 9.0 Hz), 8.38 (t, 2H, J = 8.1 Hz), 8.22 (dd, 2H, J = 8.4 and 4.8 Hz), 8.13 (dd, 8H, J = 5.1 and 1.2 Hz), 6.95 (m, 28H).

***trans*,*trans*-[Ru$_2$(16)(3,5-(CH$_3$)$_2$-py)$_4$Cl](PF$_6$)$_3$ (27g).** The same procedure as that described for **27b** was followed, using **16** (31.4 mg, 0.064 mmol), [Ru(DMSO)$_4$Cl$_2$] (73.0 mg, 0.15 mmol), and 3,5-dimethylpyridine (0.3 mL, 2.63 mmol) to afford **27g** (50 mg, 49%). Mp: >300 °C. ^{1}H NMR (acetone-d_6): δ 10.07 (dd, 2H, J = 4.2 and 2.4 Hz), 9.35 (s, 2H), 9.13 (d, 2H, J = 7.8 Hz), 8.88 (d, 4H, J = 8.4 Hz), 8.80 (dd, 2H, J = 7.8 and 1.2 Hz), 8.64 (d, 2H, J = 8.1 Hz), 8.35 (t, 2H, J = 8.4 Hz), 8.24 (dd, 2H, J = 8.4 and 4.8 Hz), 7.70 (s, 8H), 6.93 (s, 4H), 2.08 (s, 12H), 1.68 (s, 12H). Anal. Calcd for $C_{54}H_{46}ClF_{18}N_{12}O_4P_3Ru_2$: C, 43.77; H, 3.42; N, 10.56. Found: C, 44.42; H, 3.03; N, 10.08.

***trans*,*trans*-[Ru$_2$(16)(1-CH$_3$-imidazole)$_4$Cl](PF$_6$)$_3$ (28).** The same procedure as that described for **27b** was followed, using **16** (31.4 mg, 0.064 mmol), [Ru(DMSO)$_4$Cl$_2$] (73.0 mg, 0.15 mmol), and 1-methylimidazole (0.3 mL, 3.08 mmol) to afford **28** (45 mg, 47%). Mp: >300 °C. ^{1}H NMR (acetone-d_6): δ 9.88 (dd, 2H, J = 4.5 and 2.4 Hz), 9.15 (s, 2H), 8.98 (d, 2H, J = 8.7 Hz), 8.92 (d, 2H, J = 8.4 Hz), 8.88 (d, 2H, J = 7.8 Hz), 8.77 (m, 4H), 8.24 (t, 2H, J = 8.7 Hz), 8.14 (dd, 2H, J = 8.1 and 4.5 Hz), 6.95 (s, 4H), 6.53 (t, 4H, J = 1.8 Hz), 6.18 (t, 4H, J = 1.8 Hz), 3.19 (s, 12H). Anal. Calcd for $C_{46}H_{42}ClF_{18}N_{16}P_3Ru_2$: C, 37.05; H, 2.84; N, 15.02. Found: C, 37.04; H, 2.42; N, 14.71.

***trans*,*trans*-[Ru$_2$(17)(4-CH$_3$-py)$_4$Cl](PF$_6$)$_3$ (29a).** A mixture of **17** (59.0 mg, 0.10 mmol) and [Ru(DMSO)$_4$Cl$_2$] (116.2 mg, 0.24 mmol) in EtOH (60 mL) and CH_2Cl_2 (3 mL) was refluxed for 8 h, producing a dark solution. Water (8.0 mL) and 4-methylpyridine (0.4 mL, 4.1 mmol) were introduced, and the dark mixture was refluxed overnight. Et_3N (1 mL) and LiCl (20 mg) were introduced. The dark mixture was refluxed for an additional 24 h and then concentrated to about 5 mL. Addition of NH_4PF_6 (98 mg, 0.60 mmol) produced a precipitate that was purified by chromatography on alumina. The column was eluted first with hexanes/acetone (1:1) to remove the impurities, and the complex was recovered by eluting with acetone/acetonitrile/aqueous saturated KPF_6 (1:1:0.05) to afford a dark-blue solid (49 mg, 30%). Mp: >300 °C. ^{1}H NMR (acetone-d_6): δ 9.58 (m, 4H), 9.44 (s, 2H), 9.21 (d, 2H, J = 7.2 Hz), 9.08 (d, 2H, J = 9.0 Hz), 9.02 (d, 2H, J = 8.1 Hz), 8.67 (d, 2H, J = 8.7 Hz), 8.59 (d, 2H, J = 8.4 Hz), 8.52 (t, 2H, J = 7.2 Hz), 8.42 (t, 2H, J = 7.5 Hz), 8.15 (t, 2H, J = 8.1 Hz), 8.04 (d, 8H, J = 6.6 Hz), 6.45 (d, 8H, J = 6.0 Hz), 1.92 (s, 12H). MS: m/z 1491 $(M - PF_6)^+$, 1345 $(M - 2PF_6)^+$, 673 $(M - 2PF_6)^{2+}$.

***trans*,*trans*-[Ru$_2$(17)(4-CH$_3$O-py)$_4$Cl](PF$_6$)$_3$ (29b).** The same procedure as that described for **27b** was followed, using **17** (59.0 mg, 0.08 mmol), [Ru(DMSO)$_4$Cl$_2$] (93.0 mg, 0.19 mmol), and 4-methoxypyridine (0.4 mL, 3.94 mmol) to afford a dark-blue solid **29b** (39 mg, 23%). Mp: >300 °C. ^{1}H NMR (acetone-d_6): δ 9.60 (m, 4H), 9.44 (s, 2H), 9.22 (d, 2H, J = 8.1 Hz), 9.09 (d, 2H, J = 9.0 Hz), 9.05 (d, 2H, J = 7.8 Hz), 8.71 (d, 2H, J = 9.0 Hz), 8.59 (m, 4H), 8.42 (t, 2H, J = 7.8 Hz), 8.17 (t, 2H, J = 7.2 Hz), 7.97 (d, 8H, J = 6.9 Hz), 6.45 (d, 8H, J = 7.2 Hz), 3.49 (s, 12H). Anal. Calcd for $C_{62}H_{50}ClF_{18}N_{12}O_4P_3Ru_2$: C, 43.81; H, 2.97; N, 9.89. Found: C, 43.24; H, 3.08; N, 9.47.

***trans*,*trans*-[Ru$_2$(22)(4-CH$_3$-py)$_4$Cl](PF$_6$)$_3$ (30a).** The same procedure as that described for **27b** was followed, using **22** (54.0 mg, 0.10 mmol), [Ru(DMSO)$_4$Cl$_2$] (116.2 mg, 0.24 mmol), and 4-methylpyridine (0.4 mL, 4.1 mmol) to afford a dark-blue solid (70 mg, 44%). Mp: >300 °C. ^{1}H NMR (acetone-d_6): δ 10.02 (dd, 2H, J = 7.2 and 2.1 Hz), 9.52 (d, 2H, J = 8.4 Hz), 9.43 (dd, 2H, J = 6.3 and 3.0 Hz), 8.94 (d, 2H, J = 7.8 Hz), 8.86 (d, 2H, J = 7.8 Hz), 8.79 (dd, 2H, J = 7.5 and 1.5 Hz), 8.67 (d, 2H, J = 8.4 Hz), 8.47 (dd, 2H, J = 6.6 and 3.6 Hz), 8.39 (t, 2H, J = 7.8 Hz), 8.19 (dd, 2H, J = 7.5 and 3.6 Hz), 7.83 (d, 8H, J = 6.3 Hz), 6.39 (d, 8H, J = 6.3 Hz), 1.22 (s, 12H). Anal. Calcd for $C_{58}H_{48}N_{12}ClP_3F_{18}Ru_2$: C, 43.94; H, 3.05; N, 10.60. Found: C, 43.84; H, 3.02; N, 10.20.

***trans*,*trans*-[Ru$_2$(22)(4-CH$_3$O-py)$_4$Cl](PF$_6$)$_3$ (30b).** The same procedure as that described for **27b** was followed, using **22** (41.0 mg, 0.08 mmol), [Ru (DMSO)$_4$ Cl$_2$] (93.0 mg, 0.19 mmol), and 4-methoxypyridine (0.4 mL, 3.94 mmol) to afford **30b** (70 mg, 44%). Mp: >300 °C. ^{1}H NMR (acetone-d_6): δ 10.05 (dd, 2H, J = 4.5 and 2.1 Hz), 9.56 (d, 2H, J = 8.1 Hz), 9.45 (dd, 2H, J = 6.3 and 3.0 Hz), 9.00 (d, 2H, J = 7.8 Hz), 8.92 (d, 2H, J = 8.1 Hz),

8.83 (dd, 2H, J = 8.4 and 1.5 Hz), 8.75 (d, 2H, J = 9.3 Hz), 8.49 (dd, 2H, J = 6.6 and 3.0 Hz), 8.41 (t, 2H, J = 8.4 Hz), 8.23 (dd, 2H, J = 8.1 and 4.2 Hz), 7.77 (dd, 8H, J = 7.2 and 0.9 Hz), 6.15 (dd, 8H, J = 5.4 and 0.6 Hz), 3.50 (s, 12H). Anal. Calcd for $C_{58}H_{48}N_{12}O_4ClP_3F_{18}Ru_2 \cdot 2C_3H_6O$: C, 43.51; H, 3.39; N, 9.52. Found: C, 43.95; H, 3.03; N, 9.37.

***trans*,*trans*-[Ru$_2$(22)(1-CH$_3$-imidazole)$_4$Cl](PF$_6$)$_3$ (31).** The same procedure as that described for **27b** was followed, using **22** (54 mg, 0.10 mmol), [Ru(DMSO)$_4$Cl$_2$] (116.0 mg, 0.24 mmol), and l-methylimidazole (0.4 mL, 3.08 mmol) to afford **31** (50 mg, 32%). Mp: >300 °C. ^{1}H NMR (acetone-d_6): δ 9.91 (dd, 2H, J = 4.5 and 2.4 Hz), 9.41 (d, 2H, J = 8.4 Hz), 9.31 (dd, 2H, J = 9.0 and 3.0 Hz), 8.99 (d, 2H, J = 8.4 Hz), 8.88 (d, 2H, J = 9.3 Hz), 8.77 (m, 4H), 8.36 (m, 4H), 8.14 (dd, 2H, J = 7.5 and 3.6 Hz), 6.94 (s, 4H), 6.45 (t, 4H, J = 1.8 Hz), 6.05 (t, 4H, J = 1.5 Hz), 3.18 (s, 12H). Anal. Calcd for $C_{50}H_{44}ClF_{18}N_{16}O_4P_3Ru_2 \cdot 2.5(CH_3)_2CO$: C, 40.91; H, 3.49; N, 13.28. Found: C, 41.07; H, 3.17; N, 13.29.

***trans*,*trans*-[Ru$_2$(26)(4-CH$_3$-py)$_4$Cl](PF$_6$)$_3$ (32).** A mixture of **26** (43.0 mg, 0.1 mmol) and $RuCl_3 \cdot 3H_2O$ (59.3 mg, 0.23 mmol) in ethylene glycol (3 mL) was heated for 6 min in a microwave oven. EtOH/H_2O (3:1, 20 mL) and LiCl (42 mg) were added, and the mixture was heated at reflux for 7 h, after which 4-methylpyridine (320 mg) was added and reflux continued for 15 h. *N*-Methylmorpholine (0.15 mL) was added and reflux continued overnight. The mixture was poured into aqueous NH_4PF_6, and the resulting dark precipitate was collected and purified by chromatography on silica gel, eluting with CH_2Cl_2/CH_3CN. The complex **32** (43.9 mg, 30%) was obtained as a dark solid, Mp: >300 °C. ^{1}H NMR (acetone-d_6): δ 9.96 (dd, 2H, J = 4.8 and 1.5 Hz), 9.49 (s, 2H), 9.25 (d, 2H, J = 8.7 Hz), 8.79 (m, 4H), 8.35 (dd, 2H, J = 8.4 and 5.1 Hz), 8.24 (AB pattern, 4H), 7.78 (d, 8H, J = 6.6 Hz), 6.63 (d, 8H, J = 6.0 Hz), 1.99 (s, 12H). ^{13}C NMR (CD_3CN): δ 164.4, 159.7, 155.6, 151.5, 151.3, 151.1, 150.9, 139.1, 133.8, 131.6, 131.5, 129.7, 128.7, 128.4, 127.0, 126.9, 126.0, 20.8. MS: m/z 1336.5 $(M - PF_6)^+$, 596.6 $(M - 2PF_6)^{2+}$, 349.1 $(M - 3PF_6)^{3+}$.

X-ray Structure Determination of *trans*,*trans*-[Ru$_2$(22)(4-CH$_3$-py)$_4$Cl](PF$_6$)$_3$. All measurements were made with a Siemens SMART platform diffractometer equipped with a 4 K CCD APEX II detector. A hemisphere of data (1271 frames at 6 cm detector distance) was collected using a narrow-frame algorithm with scan widths of 0.30° in ω and an exposure time of 35 s/frame. The data were integrated using the Bruker-Nonius SAINT program, with the intensities corrected for Lorentz factor, polarization, air absorption, and absorption due to variation in the path length through the detector faceplate. A ψ-scan absorption correction was applied based on the entire data set. Redundant reflections were averaged. Final cell constants were refined using 7544 reflections having $I > 10\sigma(I)$, and these, along with other information pertinent to data collection and refinement, are listed in Table 4. The Laue symmetry was determined to be –1, and the space group was shown to be either $P1$ or $P\bar{1}$. The asymmetric unit consists of one cation, two anions in general positions (P1 and P2), a half-anion situated on an inversion center (P3), a half-anion in a general position (P4) shared by a disordered acetone molecule, and several other solvent molecules, which appear to be a mixture of water and acetone. The P2, P3, and P4 anions are disordered, and only the major portion of the P4 anion could be discerned. All of the solvent molecules are massively disordered and partially evacuated due to solvent loss before the X-ray data could be collected. In each location, the identity of the solvent had to be guessed. The exact amount of solvent present could only be approximated, assuming maximum occupancy at each solvent site.

Table 4. Data Collection and Processing Parameters for **30a**

compound	[Ru$_2$(**22**)(4-CH$_3$-py)$_4$Cl](PF$_6$)$_3 \cdot 2.5C_3H_6O \cdot 2H_2O$
molecular formula	$C_{65.5}H_{67}ClF_{18}N_{12}O_{4.5}P_3Ru_2$
fw	1766.81
space group	$P\bar{1}$ (triclinic)
cell constants	a = 12.4189(7) Å
	b = 15.5016(9) Å
	c = 19.7313(12) Å
	α = 88.743(1)°
	β = 74.697(1)°
	γ = 71.138(1)°
formula units per cell	Z = 2
volume	3458.7(4) Å^3
density	ρ = 1.696 g/cm^3
abs coeff	μ = 0.653 mm^{-1}
temperature	T = 223(2) K
radiation (Mo Kα)	λ = 0.710 73 Å
collection range	3.40° ≤ 2θ ≤ 47.18°
total data collected	15 611
independent data	10 256
total variables	781
R1	0.0571 with $I > 4\sigma(I)$
wR2	0.1613

Acknowledgment. We thank the Robert A. Welch Foundation (Grant E-621) and the Division of Chemical Sciences, Office of Basic Energy Sciences, U.S. Department of Energy (Contract DE-FG03-02ER15334), for financial support of this work. We also thank Dr. James Korp for assistance with the X-ray determination.

Supporting Information Available: X-ray crystallographic files for *trans*,*trans*-[Ru$_2$(**22**)(4-CH$_3$-py)$_4$Cl](PF$_6$)$_3$ in CIF format. This material is available free of charge via the Internet at http://pubs.acs.org.

IC7010875